Spera, S., & Bax, A. (1991) *J. Am. Chem. Soc. 113*, 5490–5492.
Tate, S., Kikumoto, Y., Ichikawa, S., Kaneko, M., Masui, Y., Kamogashira, T., Ouchi, M., Takahashi, S., & Inagaki, F. (1992) *Biochemistry 31*, 2435–2442.
Wingfield, P, Graber, P., Shaw, A. R., Gronenborn, A. M., Clore, G. M., & MacDonald, H. R. (1989) *Eur. J. Biochem. 179*, 565–571.
Wüthrich, K. (1986) *NMR of Proteins and Nucleic Acids*, Wiley, New York.
Zuiderweg, E. R. P., & Fesik, S. W. (1989) *Biochemistry 28*, 2387–2391.

Influence of Benzo[*a*]pyrene Diol Epoxide Chirality on Solution Conformations of DNA Covalent Adducts: The (−)-*trans-anti*-[BP]G·C Adduct Structure and Comparison with the (+)-*trans-anti*-[BP]G·C Enantiomer†

Carlos de los Santos,‡ Monique Cosman,‡ Brian E. Hingerty,§ Victor Ibanez,∥ Leonid A. Margulis,∥ Nicholas E. Geacintov,∥ Suse Broyde,⊥ and Dinshaw J. Patel*,‡

Department of Biochemistry and Molecular Biophysics, College of Physicians and Surgeons, Columbia University, New York, New York 10032, Health and Safety Research Division, Oak Ridge National Laboratory, Oak Ridge, Tennessee 37831, and Chemistry and Biology Department, New York University, New York, New York 10003

Received February 28, 1992; Revised Manuscript Received April 16, 1992

ABSTRACT: Benzo[*a*]pyrene (BP) is an environmental genotoxin, which, following metabolic activation to 7,8-diol 9,10-epoxide (BPDE) derivatives, forms covalent adducts with cellular DNA. A major fraction of adducts are derived from the binding of N^2 of guanine to the C^{10} position of BPDE. The mutagenic and carcinogenic potentials of these adducts are strongly dependent on the chirality at the four asymmetric benzylic carbon atoms. We report below on the combined NMR–energy minimization refinement characterization of the solution conformation of (−)-*trans-anti*-[BP]G positioned opposite C and flanked by G·C base pairs in the d(C1-C2-A3-T4-C5-[BP]G6-C7-T8-A9-C10-C11)·d(G12-G13-T14-A15-G16-C17-G18-A19-T20-G21-G22) duplex. Two-dimensional NMR techniques were applied to assign the exchangeable and non-exchangeable protons of the benzo[*a*]pyrenyl moiety and the nucleic acid in the modified duplex. These results establish Watson–Crick base pair alignment at the [BP]G6·C17 modification site, as well as the flanking C5·G18 and C7·G16 pairs within a regular right-handed helix. The solution structure of the (−)-*trans-anti*-[BP]G·C 11-mer duplex has been determined by incorporating intramolecular and intermolecular proton–proton distances defined by lower and upper bounds deduced from NOE buildup curves as constraints in energy minimization computations. The BP ring spans both strands of the duplex in the minor groove and is directed toward the 3′-end of the modified strand in the refined structure. One face of the BP ring of [BP]G6 stacks over the C17 residue across from it on the partner strand while the other face is exposed to solvent. The long axis of the BP ring makes an angle of approximately 40° with the average direction of the DNA helix axis and is readily accommodated within a widened minor groove of a minimally perturbed B-DNA helix. The present results on the (−)-*trans-anti*-BP-N^2-G adduct opposite C in which the BP ring is oriented toward the 3′-end of the modified strand contrast strikingly with our previous demonstration that the mirror image (+)-trans-anti stereoisomer within the same sequence context orients the BP ring toward the 5′-end of the modified strand [Cosman et al. (1992) *Proc. Natl. Acad. Sci. U.S.A. 89*, 1914–1918]. These orientational differences are due to the chiral characteristics of the two BPDE enantiomers and may have profound influences on the interaction of cellular enzyme systems with these two structurally different alignments of this bulky DNA lesion.

Chiral effects are critically important in many biological systems and interactions and are often the key factors in determining biological activity–structure relationships. Well-known examples include the metabolic stereoselective synthesis of oxygenated polycyclic aromatic derivatives (Conney, 1982; Singer & Grunberger, 1983), chiral recognition in xenobiotic metabolism and drug–receptor interactions (Testa, 1989), ligand–DNA interactions (Barton, 1989), the pharmacology of drug molecules (Campbell & Wilson, 1991), and the genotoxic, mutagenic, and tumorigenic properties of a variety of metabolites of aromatic compounds (Conney, 1982; Seiler, 1990).

A specific and extensively studied case is the stereoselective metabolism of the well-known environmental pollutant benzo[*a*]pyrene (BP) to four different benzo[*a*]pyrene-7,8-diol 9,10-epoxide stereoisomers, each of which is characterized by different mutagenic and tumorigenic activities (Conney, 1982) (Chart I). Particularly striking are the differences in the biological activities of the (+)- and (−)-enantiomers of the anti diastereomer 7β,8α-dihydroxy-9α,10α-epoxy-7,8,9,10-tetrahydrobenzo[*a*]pyrene [designated (+)-BPDE and (−)-BPDE], respectively. The (+)-BPDE enantiomer is highly tumorigenic

† This research was supported by NIH Grant CA-2111 and Columbia University Start-up Funds to D.J.P., by NIH Training Grant CA-09503 to M.C., by NIH Grant CA-20851 and DOE DE-FG02-88ER60405 Contract to N.E.G., by NIH Grant CA-28038, DOE DE-FG02-90ER60931 Contract, and NSF Grant DMB-8416009 to S.B., and by DOE DE-AC05-840R21400 Contract with Martin-Marietta Energy Systems to B.E.H.

‡ Columbia University.
§ Oak Ridge National Laboratory.
∥ Chemistry Department, New York University.
⊥ Biology Department, New York University.

0006-2960/92/0431-5245$03.00/0

Chart I

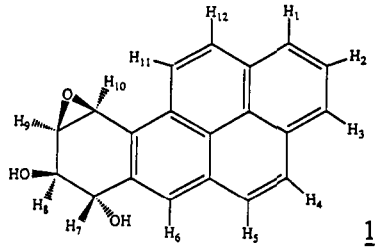

1

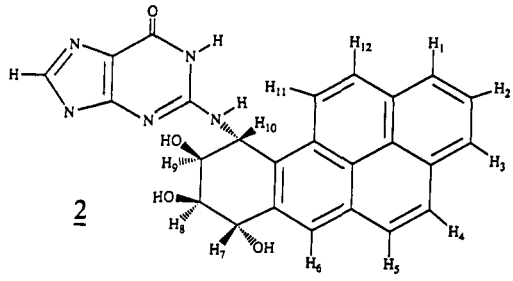

2

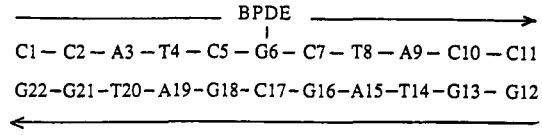

3

on mouse skin and in the newborn mouse lung system, while the (−)-BPDE isomer is not (Buening et al., 1978; Slaga et al., 1979). The (+)-enantiomer is more mutagenic in mammalian cell systems, while the (−)-BPDE is more active in bacterial cells (Wood et al., 1977; Brookes & Osborne, 1892; Stevens et al., 1985). It is widely believed that these effects are due to the formation of covalent BP diol epoxide–cellular DNA adducts (Meehan & Straub, 1979; Singer & Grunberger, 1983; Arce & Grunberger, 1983; Ashurst et al., 1983; Arce et al., 1987; Harvey & Geacintov, 1987; Cheng et al., 1989). The differences in the biological activities of the (+)- and (−)-BPDE enantiomers, which are attributed to chiral effects, have stimulated much research on the spectroscopic characteristics and low-resolution structures of the covalent adducts formed between the two BPDE enantiomers and native, double-stranded DNA (Geacintov et al., 1984; Jernstrom et al., 1984; Chen, 1985; Eriksson et al., 1988; Geacintov, 1988; Roche et al., 1989, 1991; Graslund & Jernstrom, 1989). Both enantiomers bind predominantly via the C^{10}-position of BPDE to the exocyclic amino group of guanine by cis and trans addition to the N^2 group with respect to the oxirane ring (Weinstein et al., 1976; Koreeda et al., 1976; Meehan & Straub, 1979; Cheng et al., 1989). UV-absorbance, fluorescence, and linear dichroism data obtained with (+)-BPDE- and (−)-BPDE–DNA covalent adducts suggest that two different types of covalent B-DNA binding sites can be distinguished, termed site I and II (Geacintov, 1988; Graslund & Jernstrom, 1989; Jankowiak et al., 1990; Geacintov et al., 1990; Roche et al., 1991). In site I, the pyrenyl residue is at least partially stacked with the DNA bases, and these conformations resemble, but are not identical to, intercalation sites (Geacintov et al., 1984). In site II, the pyrenyl moiety is situated at external, solvent-exposed binding sites. These spectroscopic studies have suggested that the highly tumorigenic (+)-enantiomer prefers site II binding, while the (−)-enantiomer prefers site I binding (Zinger et al., 1987; Eriksson et al., 1988). By contrast, recent studies with site-specific and stereospecific BPDE–oligonucleotide adducts suggest that both the (+)-trans and (−)-trans addition products occupy similar type II binding sites, while both (+)-cis and (−)-cis addition products prefer site I conformations (Cosman, 1991; Geacintov et al., 1990, 1991). In the present work, high-resolution NMR combined with energy minimization techniques are used to elucidate the solution conformation of a (−)-*anti*-BP–N^2-G adduct positioned opposite C and flanked by G·C base pairs in an 11-mer deoxyoligonucleotide duplex. This structure is compared to the conformation of a (+)-*anti*-BP–N^2-G adduct in the same DNA sequence context derived earlier (Cosman et al., 1992).

Materials and Methods

Preparation of the (−)-trans-anti-[BP]G·C 11-mer Duplex. Racemic BPDE was purchased from the National Cancer Institute Chemical Carcinogenic Reference Standard Repository. The synthesis of the [BP]G covalent adduct in the d(C-C-A-T-C-[BP]G-C-T-A-C-C) sequence was carried out starting from racemic *anti*-BPDE using previously described methods (Cosman et al., 1990, 1992). The (−)-*trans-anti*-BP–N^2-G containing 11-mer was separable from the (+)-trans, (+)-cis, and (−)-cis isomeric adducts by preparative HPLC on a C_{18} ODS Hypersil column. The oligomer sequence was degraded with snake venom phosphodiesterase and bacterial alkaline phosphatase to characterize and verify the base composition of the modified oligomer. The modified enantiomerically pure d(C-C-A-T-C-[BP]G-C-T-A-C-C) strand was annealed to its complementary unmodified d(G-G-T-A-G-C-G-A-T-G-G) strand at 65 °C, and the stoichiometry was followed by monitoring single proton resonances in both strands.

NMR Experiments. A combination of through-space nuclear Overhauser effect and through-bond correlated two-dimensional spectra was recorded and analyzed to assign the carcinogen and nucleic acid protons in the (−)-*trans-anti*-[BP]G·C 11-mer duplex. NOESY data sets on the modified duplex in H_2O buffer at 5 °C were recorded at a mixing time of 200 ms using a jump–return pulse for solvent suppression while the corresponding NOESY spectra in D_2O buffer at 25 °C were recorded at a mixing time of 300 ms. The through-bond HOHAHA data sets in D_2O buffer at 25 °C were recorded at spin lock times of 50, 80, and 120 ms.

The NOE buildup curves involving nonexchangeable protons were based on NOESY data sets on the modified duplex in D_2O buffer at 25 °C recorded at mixing times of 50, 90, 130, 170, and 210 ms. The slope of the volume integrals of the resolved cross-peaks at short mixing times was used to estimate the distance constraints defined by lower and upper bounds using the fixed cytidine H6–H5 2.45-Å separation as the reference distance.

The proton–proton vicinal coupling constants among sugar protons were analyzed from phase-sensitive COSY and DQF-COSY spectra and used to qualitatively distinguish between the C3′-endo and C2′-endo family of sugar puckers in the (−)-*trans-anti*-[BP]G·C 11-mer duplex. The relative intensity of the NOE cross-peaks between base protons and their own and 5′-flanking sugar H2′, H2″, and H3′ protons was used to qualitatively distinguish between the A and B family of helices for the modified duplex (van der Ven & Hilbers, 1988).

Energy Minimization Computations. DUPLEX is a molecular mechanics program for nucleic acids that performs potential energy minimizations in the reduced variable domain of torsion angle space (Hingerty et al., 1989). The vast diminution in the number of variables that must be simultaneously optimized, compared to Cartesian space minimizations, permits large

movements from a given starting conformation during minimization. It has the option of including distance constraints through penalty functions to compute structures that are minimum energy conformations (Norman et al., 1989). Details of the force fields and parametrization have been published previously (Hingerty et al., 1989). Details about the functions employed to search for structures within the NMR-defined distance bounds were given in an earlier publication (Schlick et al., 1990). The penalty functions are released in terminal minimizations to yield unconstrained structures that are energy minima and within the range of the NMR data.

Results

Exchangeable Proton Spectra. The exchangeable proton spectrum (12.3–14.2 and 7.2–9.4 ppm) of the (−)-*trans-anti*-[BP]G·C 11-mer duplex in H_2O buffer, pH 7.0 at 5 °C, is plotted in Figure 1A. We detect partially resolved imino protons between 12.5 and 14.0 ppm and a resolved exchangeable proton at 9.04 ppm in the spectrum. The imino and amino protons have been assigned by standard procedures [reviewed in Patel et al. (1987) and van de Ven and Hilbers (1988)] following analysis of the NOESY (200-ms mixing time) contour plot of the duplex in H_2O buffer recorded at 5 °C. The thymidine imino protons exhibit NOEs to adenosine H2 protons (cross-peaks in box I, Figure 1B), and the guanosine imino protons exhibit NOEs to the hydrogen-bonded cytidine amino protons (cross-peaks in box II, Figure 1B). These NOE patterns establish that all A·T and G·C base pairs including C5·G18 (peak I, Figure 1B) and C7·G16 (peak H, Figure 1B) adopt Watson–Crick alignment in the (−)-*trans-anti*-[BP]G·C 11-mer duplex.

There are several NOEs that define structural features for the C5-[BP]G6-C7·G16-C17-G18 segment centered about the covalent lesion site. We detect a strong NOE between the 13.22-ppm imino and 9.04-ppm downfield-shifted amino protons (peak C, Figure 1B), permitting assignment of these protons to the guanosine imino and amino protons of [BP]G6 in the duplex. Further, the imino proton of [BP]G6 exhibits an NOE to the hydrogen-bonded amino proton of C17 (peak F, Figure 1B), establishing that [BP]G6 pairs with C17 through Watson–Crick alignment. The observed NOEs between imino protons on adjacent base pairs establish that the [BP]G6·C17 pair stacks over the C5·G18 pair in one direction (peak B, Figure 1B) and the C7·G16 pair in the other direction (peak A, Figure 1B) in the duplex.

These results establish that the central C5-[BP]G6-C7·G16-C17-G18 trinucleotide adopts a base-paired stacked helical segment despite insertion of the (−)-*anti-trans*-BP-N^2-G adduct positioned opposite C in the duplex. In addition, the one-dimensional (Figure 1A) and two-dimensional (Figure 1B) exchangeable proton data are consistent with formation of a single conformation for the (−)-*trans-anti*-[BP]G·C 11-mer duplex in solution.

Nonexchangeable Proton Spectra. Expanded regions of the nonexchangeable proton spectrum of the (−)-*trans-anti*-[BP]G·C 11-mer duplex in D_2O buffer, pH 7.0 at 25 °C, are plotted in Figure 2A. The proton spectrum exhibits well-resolved resonances as can be seen for the aromatic (6.6–8.5 ppm) and sugar H1′ (5.3–6.5 ppm) proton regions in the modified duplex (Figure 2A). The base and sugar protons (except superpositioned H5′,5″ protons) have been completely assigned following analysis of NOESY, DQF-COSY, and HOHAHA spectra based on standard nucleic acid assignment procedures [Hare et al., 1983; reviewed in Reid (1987)].

Expanded NOESY (300-ms mixing time) contour plots

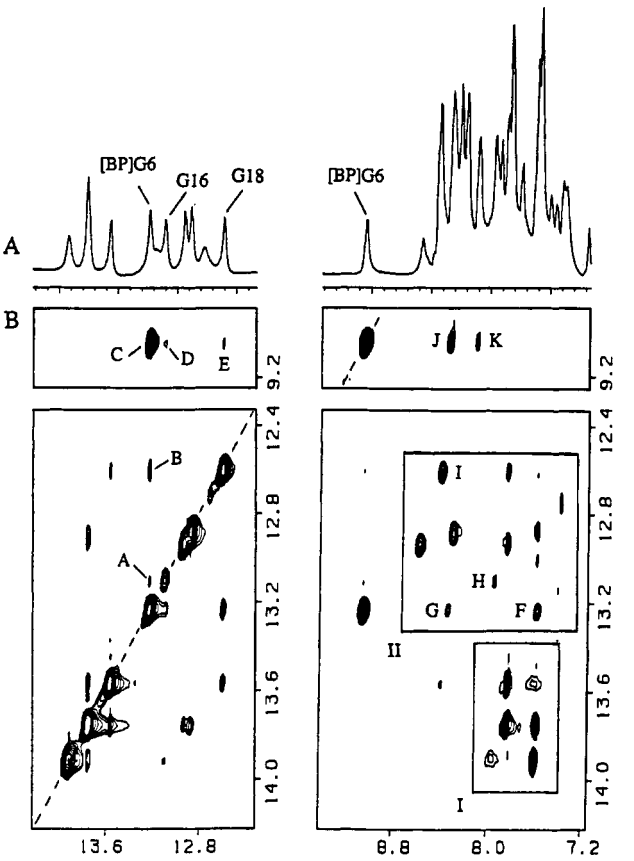

FIGURE 1: (A) Proton NMR spectrum (12.3–14.2 and 7.2–9.4 ppm) of the (−)-*trans-anti*-[BP]G·C 11-mer duplex in 0.1 M NaCl, 10 mM phosphate, and H_2O, pH 7.0 at 5 °C. The guanosine imino and amino proton assignments for the [BP]G6·C17 modification site and the guanosine imino proton assignments of the flanking C5·G18 and C7·G16 base pairs are assigned over the spectrum. (B) Expanded NOESY (200-ms mixing time) contour plots establishing distance connectivities (left panel) in the symmetrical 12.3–14.2-ppm imino proton region and (right panel) between the imino protons and the 7.2–9.4-ppm base and amino proton region. The boxed region I exhibits NOE cross-peaks between the thymidine imino protons and adenosine H2 protons in Watson–Crick base pairs. The boxed region II exhibits NOE cross-peaks between the guanosine imino protons and hydrogen-bonded cytidine amino protons in Watson–Crick G·C base pairs. Cross-peaks A–K are assigned as follows: A, [BP]G6-(NH1)–G16(NH1); B, [BP]G6(NH1)–G18(NH1); C, [BP]G6-(NH1)–[BP]G6(NH2); D, G16(NH1)–[BP]G6(NH2); E, G18-(NH1)–[BP]G6(NH2); F, [BP]G6(NH1)–C17(NH4); G, [BP]-G6(NH1)–BP(H11); H, G16(NH1)–C7(NH4); I, G18(NH1)–C5-(NH4); J, [BP]G6(NH2)–BP(H11); K, [BP]G6(NH2)–BP(H12).

correlating distance connectivities between the base and the sugar H1′ protons in the modified duplex in D_2O buffer at 25 °C are plotted in Figure 2B. The connectivities between base (purine H8 or pyrimidine H6) protons and their own and 5′-flanking sugar H1′ protons can be traced for the T4-C5-[BP]G6-C7-T8 segment on the modified strand (solid lines, Figure 2B) and for the A15-G16-C17-G18-A19 segment on the unmodified strand (dashed lines, Figure 2B). The directionality of these NOE connectivities establishes a right-handed alignment for the T4-C5-[BP]G6-C7-T8·A15-G16-C17-G18-A19 segment centered about the modified site.

Several base and sugar H1′ proton chemical shifts resonate outside their normal range in the modified duplex. Thus, the H6 of C17 resonates at 6.64 ppm compared to an average value of 7.4 ppm for other cytidines while the H1′ of C17 is shifted dramatically upfield to 2.74 ppm compared to an average value of 5.9 ppm for the other cytidines in the modified duplex (Figure 2B). In addition, the H1′ proton of [BP]G6 and C7 are shifted downfield while the H1′ protons of G16

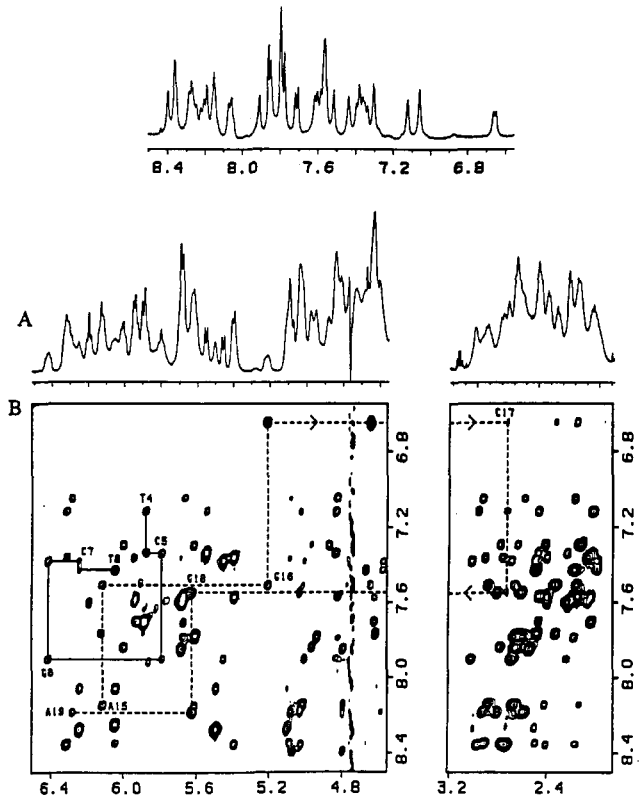

FIGURE 2: (A) Proton NMR spectrum (6.6–8.5, 4.6–6.5, and 1.9–3.2 ppm) of the (−)-*trans-anti*-[BP]G·C 11-mer duplex in 0.1 M NaCl, 10 mM phosphate, and D_2O, pH 7.0 at 25 °C. (B) Expanded NOESY (300-ms mixing time) contour plot establishing distance connectivities between the 6.6–8.5-ppm base protons and the 4.6–6.5- and 1.9–3.2-ppm sugar protons. The solid lines trace connectivities between the base protons and its own and 5′-flanking sugar H1′ protons in the T4-C5-[BP]G6-C7-T8 segment in the modified strand while the dashed line follows the connectivities in the A15-G16-C17-G18-A19 segment in the unmodified strand.

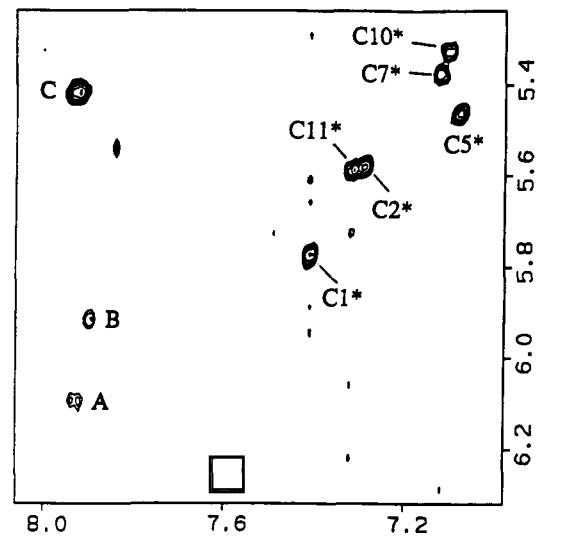

FIGURE 3: An expanded NOESY (50-ms mixing time) contour plot establishing distance connectivities between 7.1–8.4 and 5.2–6.5 ppm in the (−)-*anti-trans*-[BP]G·C 11-mer duplex in 0.1 M NaCl, 10 mM phosphate, and D_2O, pH 7.0 at 25 °C. The NOEs between the 2.45-Å fixed distance H6 and H5 of cytidines are designated by asterisks. The boxed region corresponds to the NOE between the [BP]G6(H8) and [BP]G6(H1′) protons which is too weak to detect at this mixing time. NOE cross-peaks A–C are assigned as follows: A, C7-(H1′)–BP(H11); B, T8(H1′)–BP(H1); C, BP(H10)–BP(H11). The BP pyrenyl protons (8.05–8.4 ppm) and benzylic protons (4.1–5.5 ppm) have been assigned on the basis of the observed through-bond and through-space connectivities. These assignments in the (−)-*trans-anti*-[BP]G·C 11-mer duplex are as follows: BP(H1), 8.24 ppm; BP(H2,H12), 8.05 ppm; BP(H3), 8.27 ppm; BP(H4), 8.21 ppm; BP(H5), 8.14 ppm; BP(H6), 8.39 ppm; BP(H7), 5.08 ppm: BP(H8), 4.17 ppm; BP(H9), 5.11 ppm; BP(H10), 5.50 ppm.

and to a lesser extent G18 are shifted upfield in the modified duplex (Figure 2B). The observed upfield shifts for the minor groove sugar H1′ protons of G16 and most dramatically C17 suggest that the aromatic pyrenyl ring of [BP]G6 stacks over the G16-C17 on the partner strand in the minor groove and is directed toward the 3′-end of the modified strand in the (−)-*trans-anti*-[BP]G·C 11-mer duplex. These results are in striking contrast to the large upfield shifts of the sugar H1′ protons of G18 and A19 in the (+)-*trans-anti*-[BP]G·C 11-mer duplex where the aromatic pyrenyl ring of [BP]G6 is directed toward the 5′-end of the modified strand (Cosman et al., 1992).

The anti or syn orientation about the [BP]G6 glycosidic bond in the (−)-*trans-anti*-[BP]G·C 11-mer duplex has been probed by recording the NOESY spectrum in D_2O at a short mixing time of 50 ms. We do not detect the NOE cross-peak between the H8 and H1′ protons of [BP]G6 (see box, Figure 3B) compared to the clearly detectable NOEs between the H6 and H5 of cytidines (designated by asterisks in Figure 3B; the fixed interproton separation is 2.45 Å) in the duplex. This result establishes that [BP]G6 adopts an anti glycosidic torsion angle since the base to sugar H1′ NOE would be comparable in intensity to the cytidine H6-H5 NOE if the glycosidic torsion angle were syn as seen for guanines in Z-DNA (Patel et al., 1982) and in exocyclic adducts of guanine (Kouchakdjian et al., 1989) and adenine (de los Santos et al., 1991) at the duplex level.

A qualitative analysis of sugar proton coupling constants and the intensity of the base proton to sugar H2′, H2″, and H3′ proton NOEs at short mixing times establishes that the sugar puckers at and adjacent to the [BP]G6·C17 lesion site adopt C2′-endo sugar puckers characteristic of B-DNA helices in the (−)-*trans-anti*-[BP]G·C 11-mer duplex.

The aromatic (8.0–8.3 ppm) and aliphatic (4.2–5.5 ppm) protons of the BP ring in the (−)-*trans-anti*-[BP]G·C 11-mer duplex have been completely assigned following analysis of the intramolecular NOE patterns and coupling connectivities around the BP ring. These assignments are listed in the caption to Figure 4 and provide the necessary markers to monitor intermolecular NOEs in the modified duplex.

Intermolecular NOEs. A total of 27 intermolecular NOEs (of which 9 involve exchangeable nucleic acid protons) have been identified and assigned in the NOESY spectrum of the (−)-*trans-anti*-[BP]G·C 11-mer duplex. Several of these intermolecular NOEs are labeled in expanded NOESY plots in Figure 4 with the cross-peak assignments listed in the figure caption. The 6 intermolecular NOEs involving the BP benzylic protons are between the H9, H10 protons of BP and the minor groove (H1′ and NH_2) protons of the [BP]G6-C7 step in the modified strand at the covalent linkage site.

The 21 intermolecular NOEs involving the BP pyrenyl protons can be classified into those involving the H11, H12 protons, the H4, H5, H6 protons, and the H1, H2, H3 protons representing the different edges of the aromatic ring system. The H11, H12 protons of BP exhibit NOEs to the minor groove sugar (H1′ and H4′) protons of the C7-T8 step in the modified strand while the H4, H5, H6 protons exhibit NOEs to the minor groove sugar protons of the C17-G18 step in the unmodified strand. We also detect NOEs between the H2, H3 protons of BP and the minor groove sugar proton of C17 in the (−)-*trans-anti*-[BP]G·C 11-mer duplex. These results establish that the BP ring is positioned in the minor groove with different edges of the pyrenyl ring interacting with the

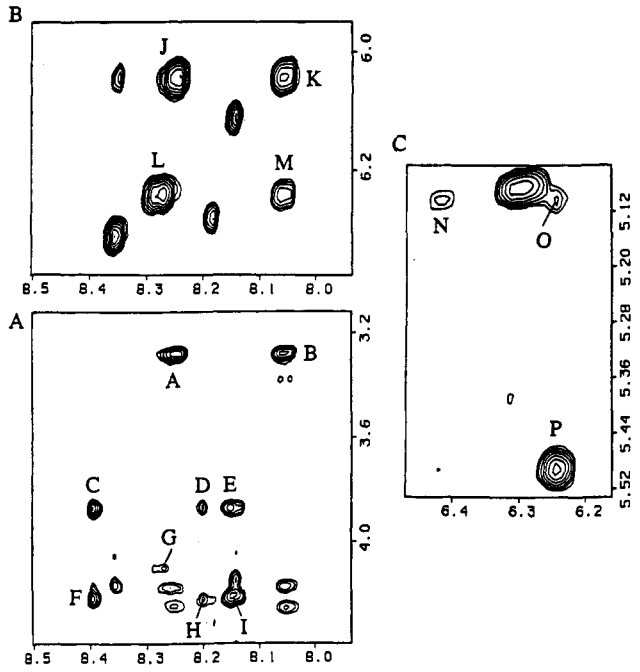

FIGURE 4: Expanded NOESY (300-ms mixing time) contour plots establishing distance connectivities (A) between the 3.1–4.4 and 7.9–8.5-ppm regions, (B) between the 6.0–6.4 and 7.9–8.5-ppm regions, and (C) between the 5.0–5.5 and 6.1–6.5-ppm regions in the (−)-*trans-anti*-[BP]G·C 11-mer duplex in 0.1 M NaCl, 10 mM phosphate, and D_2O, pH 7.0 at 25 °C. Cross-peaks A–I are assigned as follows: A, T8(H4′)–BP(H1); B, T8(H4′)–BP(H2); C, G18(H5′/H5″)–BP(H6); D, G18(H5′/H5″)–BP(H4); E, G18(H5′/H5″)–BP(H5); F, G18(H5′/H5″)–BP(H6); G, C7(H4′)–BP(H11); H, G18(H5′/H5″)–BP(H4); I, G18(H5′/H5″)–BP(H5). Cross-peaks J–M are assigned as follows: J, T8(H1′)–BP(H1); K, T8(H1′)–BP(H2); L, C7(H1′)–BP(H11); M, C7(H1′)–BP(H12). Cross-peaks N–P are assigned as follows: N, BP(H9)–G6(H1′); O, BP(H9)–C7(H1′); P, BP(H10)–C7(H1′).

C7-T8 step on the modified strand and the C17-G18 step on the unmodified strand.

Most importantly, the intermediate to strong intermolecular NOEs between the H1′ proton of T8 and the H1 proton of BP (peak J, Figure 4B) and the H2 proton of BP (peak K, Figure 4B) establish that the long axis of the benzo[*a*]pyrene ring is directed toward the 3′-end of the modified strand in the (−)-*trans-anti*-[BP]G·C 11-mer duplex.

Energy Minimization Computations. Previous computational studies have addressed the conformation of the (−)-*trans-anti*-[BP]G·C adduct embedded in an alternating d(G-C)$_6$·d(G-C)$_6$ duplex (Singh et al., 1991). The approach employed involved conformational searches with potential energy minimization calculations using the DUPLEX program (see Materials and Methods) on the C-[BP]G and the C-[BP]G-C segments, followed by energy-minimized buildup techniques which position the (−)-*trans-anti*-[BP]G opposite C at the DNA oligomer duplex level. These search and build efforts yielded two distinct low-energy conformations. One of these conformations requires that the [BP]G adopts a syn glycosidic torsion angle orientation and places the BP ring in the major groove (Singh et al., 1991). This conformation can be eliminated from further consideration since the NMR data require that [BP]G6 adopt an anti orientation and the BP ring be positioned in the minor groove of the (−)-*trans-anti*-[BP]G·C 11-mer duplex.

The other of these computed conformations retains the anti orientation about the [BP]G6 glycosidic bond and directs the long axis of the BP pyrenyl ring toward the 3′-end of the modified strand in the minor groove (Singh et al., 1991). This latter conformation which is in qualitative agreement with the NMR data serves as a starting model following base sequence and length adjustment for energy minimization computations which incorporate the proton–proton distance constraints defined by lower and upper bounds from NOE buildup curves on the (−)-*trans-anti*-[BP]G·C 11-mer duplex. The available intramolecular and intermolecular distance bounds were constrained within the limits using penalty functions during the energy minimization with the DUPLEX program as described previously (Norman et al., 1989). The hydroxyl groups of the benzylic ring of BPDE were fixed in the observed 7,8-diequatorial 9,10-diaxial conformation (Neidle et al., 1982) during the constrained energy minimization computations. The starting structure readily converged to its energy-minimized counterpart that satisfied the experimental distance constraints with an rmsd between structures of 0.27 Å for the central d(T4-C5-[BP]G6-C7-T8)·d(A15-G16-C17-G18-A19) five-base-pair segment of the (−)-*trans-anti*-[BP]G·C 11-mer duplex. A very similar structure was obtained after release of all constraints, with the rmsd from the constrained structure for this central segment of 0.30 Å. Convergence was also observed to essentially the same final structure even for starting structures that differ by 45° at each of the two bonds at the base–carcinogen linkage site in the (−)-*trans-anti*-[BP]G·C 11-mer duplex.

Solution Structure. Stereoviews of the central d(T4-C5-[BP]G6-C7-T8)·d(A15-G16-C17-G18-A19) segment of the final energy-minimized structure of the (−)-*anti-trans*-[BP]G·C 11-mer duplex are shown in Figures 5A and 6A, respectively. The pyrenyl moiety in dark is directed toward the 3′-end of the modified strand and makes an angle of approximately 40° with the average helix axis (Figure 5A); the values of 37–45° previously established by linear dichroism techniques for site II (trans) adducts derived from the binding of (−)-BPDE to native DNA (Geacintov et al., 1984) are in remarkable agreement with this result. The pyrenyl moiety of [BP]G6 is positioned in the minor groove with one face stacked over the sugar of C17 on the partner strand while the other face is exposed to solvent (Figure 6A). This orientation is defined by torsion angles of 152° at the N^1–C^2–N^2–C^{10} and 78° at the C^2–N^2–C^{10}–C^9 at the base–carcinogen linkage site for the (−)-*trans-anti*-[BP]G·C 11-mer duplex.

There is a widening of the minor groove of the DNA duplex in the internal segment centered about the covalent modification site in the (−)-*trans-anti*-[BP]G·C 11-mer duplex. (The shortest phosphorus–phosphorus separation across the minor groove increases from ~4 Å toward either end of the helix to 8.1 Å toward the center of the helix).

Otherwise, the helix is quite regular with Watson–Crick pairing alignments at all base pairs including the [BP]G6·C17 pair at the modification site, all glycosidic torsion angles are in the anti range (values distributed between −100° and −127°), and all sugar puckers are in the C1′-exo/C2′-endo range (values distributed between 130° and 165°) (Figures 5A and 6A). The averagle helical twist angle for the central five-base-paired segment is 36.7° in the computed structure, and the backbone torsion angles are in the B_I family of DNA helical structures.

DISCUSSION

NMR Spectral Quality. We have observed narrow proton spectra (Figures 1A and 2A) for the (−)-*trans-anti*-[BP]G·C 11-mer duplex containing an enantiomerically pure BPDE-N^2-G positioned opposite C in the center of the helix. The proton resonances of the central T4-C5-[BP]G6-C7-T8·A15-G16-C17-G18-A19 segment are well resolved and amenable

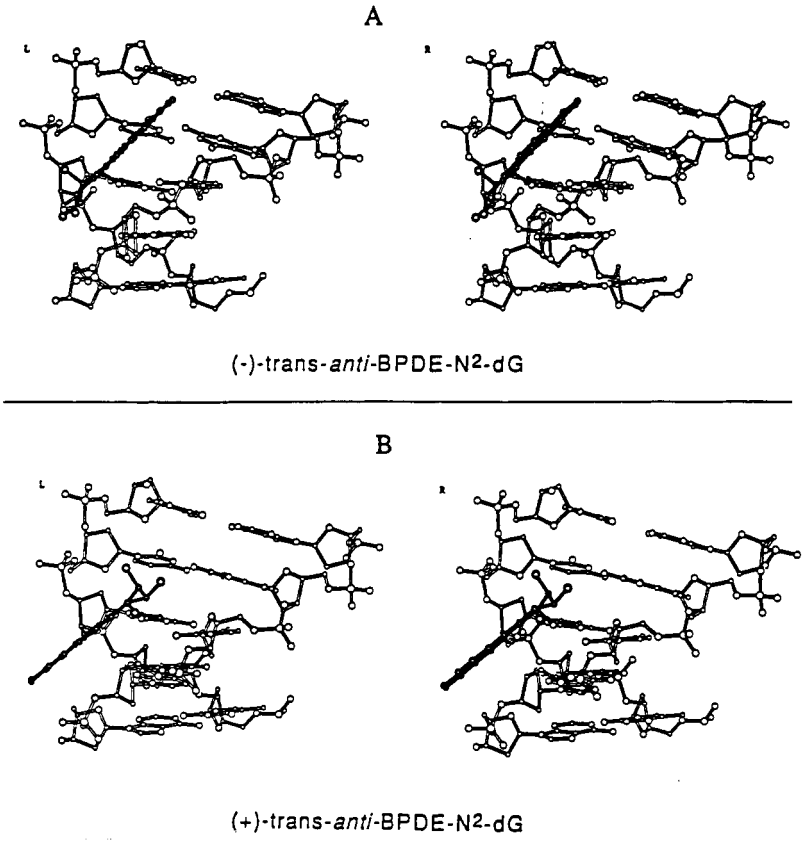

FIGURE 5: Stereo pairs of the T4-C5-[BP]G6-C7-T8·A15-G16-C17-G18-A19 segment in the solution structure of (A) the (−)-*trans-anti*-[BP]G·C 11-mer duplex and (B) the (+)-*trans-anti*-[BP]G·C 11-mer duplex. The BP ring is shown with darkened bonds, and these views emphasize the inclination between the BP long axis and the DNA helix axis. T8 is the base in the upper left-hand corner while A15 is the base in the upper right-hand corner for this view. The long axis of the BP ring is directed toward the 3′-end of the modified strand for the (−)-*trans-anti*-[BP]G6·C17 adduct in (A) and is directed toward the 5′-end of the modified strand for the (+)-*trans-anti*-[BP]G6·C17 adduct in (B).

to further characterization by two-dimensional NMR measurements. The complete assignment of the BP protons, as well as the base and sugar H1′, H2′,2″, H3′, and H4′ protons, permits, in turn, the identification of the intermolecular NOEs so critical for establishing the alignment of BP along the DNA helix. Further, several base and sugar resonances of the segment centered about the modification site exhibit unusually shifted resonances as a consequence of experiencing the ring current contributions associated with the aromatic pyrene ring of [BP]G6 in the modified duplex.

Structural Conclusions. The combined NMR energy minimization studies unequivocally establish that the BP ring of the (−)-*trans-anti*-BP-N^2-G6 adduct is positioned in the minor groove, spans both strands of the duplex, and is directed toward the 3′-end of the modified strand (Figures 5A and 6A). We detect Watson–Crick pairing at all A·T and G·C pairs, as well as the [BP]G6·C17 pair at the modification site, and the directionally and magnitude of the NOEs between the base and their own and flanking sugar protons are consistent with a right-handed helix in the B-DNA family for the modified duplex.

The glycosidic torsion angle is anti for the (−)-*trans-anti*-BP-N^2-G6 positioned opposite C17 in the modified strand and rules out models that consider a syn glycosidic torsion angle and positioning of BP in the major groove (Singh et al., 1991). On the other hand, the NMR experimental distance constraints are consistent with the energy-minimized minor groove binding model of (−)-*trans-anti*-BP-N^2-G positioned opposite C in a DNA duplex (Singh et al., 1991).

The final refined structure predicts that the BP ring in the minor groove stacks directly over the sugar of C17 (Figure 6A), and this overlap feature is strongly supported both by the observed intermolecular NOEs and by the large upfield shifts of the minor groove sugar protons of C17 in the modified duplex. The widened minor groove readily accommodates the (−)-*trans-anti*-BPDE covalently attached to the N^2 of G6 with the long axis of the pyrene ring inclined by approximately 40° relative to the long axis of the helix.

Chirality of BPDE, Adduct Orientations, and Carcinogenic Potential. It is of interest to compare the alignment of the (−)-*trans-anti*-BP-N^2-G6 adduct opposite C17 in the T4-C5-[BP]G6-C7-T8·A15-G16-C17-G18-A19 segment reported in this study (Figures 5A and 6A) with the corresponding alignment of the mirror image (+)-*trans*-anti-BP-N^2-G6 adduct opposite C17 in the same sequence context studied previously from our laboratory (Figures 5B and 6B). We note that both adducts are positioned in a widened minor groove of a minimally perturbed B-DNA helix but have the pyrenyl ring systems pointed in opposite directions. Both lesions can be identified from their absorbance, CD, and fluoresence spectroscopic properties as site II adducts, and their characteristics are strikingly different from site I cis adducts (Cosman, 1991; Geacintov et al., 1992). Upon trans addition of N^2-G to the BPDE C^{10} position, opposite orientations of the pyrenyl moieties are favored in the present sequence context. A full understanding of this effect of BPDE chirality awaits further characterization.

It has been proposed that site II adducts are associated with higher tumorigenic potentials than site I adducts (Geacintov, 1988). However, neither the tumorigenic nor mutagenic potentials of the (+)- and (−)-*trans*- (site II) and (+)- and (−)-*cis*- (site I) BP-N^2-G lesions have been explicitly established so far. It is clear from our results that the orientational properties of site II (+)-*trans*- and site II (−)-*trans*-BP-N^2-G

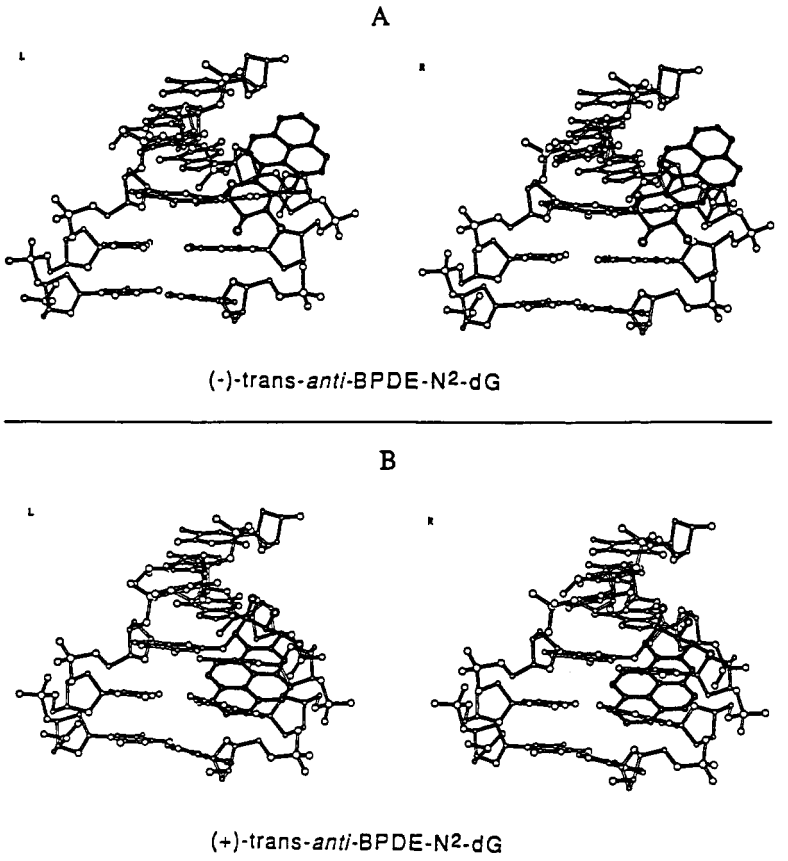

FIGURE 6: Stereo pairs of the T4-C5-[BP]G6-C7-T8·A15-G16-C17-G18-A19 segment in the solution structure of the (A) (−)-*trans-anti*-[BP])G·C 11-mer duplex and (B) (+)-*trans-anti*-[BP]G·C 11-mer duplex. The BP ring is shown with darkened bonds with this view looking into the minor groove. It also emphasizes the difference between the two faces of the BP ring. One face forms van der Waals contacts with the sugar–phosphate backbone on the partner strand while the other face is exposed to solvent. T4 is the base in the lower left-hand corner while A19 is the base in the lower right-hand corner. The BP ring stacks over C17 for the (−)-*trans-anti*-[BP]G6·C17 adduct in (A) and over G18 for the (+)-*trans-anti*-[BP]G6·C17 adduct in (B).

adducts are remarkably different from one another and that these structural effects could result in profound differences in biological activities. The long axis of the pyrenyl residue (a vector drawn between the 2 and 7 positions of BPDE) makes an angle of 40–45° with the average helical axis in both adducts with the important distinction that the pyrenyl ring is directed toward the 3′-end of the modified strand in the (−)-*trans*-BP-N^2-G adduct (Figure 5A), while it is directed toward the 5′-end of the modified strand in the (+)-*trans*-BP-N^2-G adduct (Figure 5B). This directionality of the covalently linked carcinogen could account, in part, for the differences in the mutagenic potentials of the BPDE enantiomers. For example, the reversed order of mutagenicities observed in mammalian and in bacterial cells (Wood et al., 1977; Brookes & Osborne, 1982; Stevens et al., 1985) attributed to differences in the cellular processing of these lesions (Stevens et al., 1985) could be due to differences in recognition of these two types of lesions by repair enzymes and/or the replication machinery. Obviously, superimposed on any differences in the biological activities of the size II (+)-*trans*- and (−)-*trans*-BP-N^2-G lesions are (1) differences in the yields of trans and cis N^2-G products and differences in their mutagenic specificities and potentials and (2) the generation of other minor, but potentially biologically important lesions which arise when (+)- and (−)-BPDE react with cellular DNA (Cheng et al., 1988).

This contribution briefly outlines the main conclusions of the NMR–energy minimization studies of the (−)-*trans-anti*-(BP)G·C 11-mer duplex and compares these results with parallel studies on the (+)-*trans-anti*-(BP)G·C 11-mer duplex reported earlier (Cosman et al., 1992). A detailed account of proton, carbon, and phosphorus NMR assignments and distance and coupling constant constraints, as well as back-calculation computations using molecular dynamics algorithms, will be described elsewhere on both duplexes on completion of ongoing experiments.

ACKNOWLEDGMENTS

Computations were carried out on the Cray supercomputers at the DOE's National Energy Research Supercomputer Center and the NSF's San Diego Supercomputing Center. S.B. thanks Dr. Suresh Singh for his assistance in performing some of the computations.

REFERENCES

Arce, G. T., & Grunberger, D. (1983) *Mutat. Res. 109*, 183–193.

Arce, G. T., Allen, J. W., Doerr, C. L., Elmore, E., Hatch, G. G., Moore, M. M., Sharief, Y., Grunberger, D., & Nesnow, S. (1987) *Cancer Res. 47*, 3388–3395.

Ashurst, S. W., Cohen, G. M., Nesnow, S., DiGiovanni, J., & Slaga, T. J. (1983) *Cancer Res. 43*, 1024–1029.

Barton, J. K. (1989) *Pure Appl. Chem. 61*, 563–564.

Brookes, P., & Osborne, M. R. (1982) *Carcinogenesis 3*, 1223–1226.

Buening, M. K., Wislocki, P. G., Levin, W., Yagi, H., Thakker, D. R., Akagi, H., Koreeda, M., Jerina, D. M., & Conney, A. H. (1978) *Proc. Natl. Acad. Sci. U.S.A. 75*, 5358–5361.

Campbell, D. B., & Wilson, K. (1991) *Biochem. Soc. Trans. 119*, 472–475.

Chen, F. M. (1985) *Biochemistry 24*, 6219–6227.

Cheng, S. C., Hilton, B. D., Roman, J. M., & Dipple, A. (1989) *Chem. Res. Toxicol. 2*, 334–340.

Conney, A. H. (1982) *Cancer Res. 42*, 4875–4917.
Cosman, M. (1991) Ph.D. Dissertation, New York University, New York.
Cosman, M., Ibanez, V., Geacintov, N. E., & Harvey, R. G. (1990) *Carcinogenesis 11*, 1667–1672.
Cosman, M., de los Santos, C., Fiala, R., Hingerty, B. E., Singh, S. B., Ibanez, V., Margulis, L. A., Live, D., Geacintov, N. E., Broyde, S., & Patel, D. J. (1992) *Proc. Natl. Acad. Sci. U.S.A. 89*, 1914–1918.
De los Santos, C., Kouchakdjian, M., Yarema, K., Basu, A., Essigmann, J., & Patel, D. J. (1991) *Biochemistry 30*, 1828–1835.
Eriksson, M., Norden, B., Jernstrom, B., & Graslund, A. (1988) *Biochemistry 27*, 1213–1221.
Geacintov, N. E. (1988) in *Polycyclic Aromatic Hydrocarbon Carcinogenesis: Structure–Activity Relationships* (Yang, S. K., & Silverman, B. D., Eds.) Vol. II, pp 181–206, CRC Press, Boca Raton, FL.
Geacintov, N. E., Ibanez, V., Gagliano, A. G., Jacobs, S. A., & Harvey, R. G. (1984) *J. Biomol. Struct. Dyn. 1*, 1473–1484.
Geacintov, N. E., Cosman, M., Ibanez, V., Birke, S. S., & Swenberg, C. E. (1990) in *Molecular Basis of Specificity in Nucleic Acid–Drug Interactions* (Pullman, B., & Jortner, J., Eds.) pp 433–450, Kluwer Academic Publishers, Dordrecht, The Netherlands.
Geacintov, N. E., Cosman, M., Mao, B., Alfano, A., Ibanez, V., & Harvey, R. G. (1991) *Carcinogenesis 12*, 2099–2108.
Graslund, A., & Jernstrom, B. (1989) *Q. Rev. Biophys. 22*, 1–37.
Hare, D. R., Wemmer, D. E., Chou, S. H., Drobny, G., & Reid, B. R. (1983) *J. Mol. Biol. 171*, 319–336.
Harvey, R. G., & Geacintov, N. E. (1988) *Acc. Chem. Res. 21*, 66–73.
Hingerty, B. E., Figueroa, S., Hayden, T., & Broyde, S. (1989) *Biopolymers 28*, 1195–1222.
Jankowiak, R., Lu, P.-Q., Small, G., & Geacintov, N. E. (1990) *Chem. Res. Toxicol. 3*, 39–46.
Jernstrom, B., Lycksell, P.-O., Graslund, A., & Norden, B. (1984) *Carcinogenesis 5*, 1129–1135.
Koreeda, M., Moore, P. D., Wislocki, P. G., Levin, W., Conney, A. H., Yagi, H., & Jerina, D. M. (1978) *Science 199*, 778–781.
Kouchakdjian, M., Marinelli, E., Gao, X., Johnson, F., Grollman, A., & Patel, D. J. (1989) *Biochemistry 28*, 5647–5657.
Meehan, T., & Straub, K. (1979) *Nature 277*, 410–412.
Neidle, S., Subbiah, A., Kuroda, R., & Cooper, C. S. (1982) *Cancer Res. 42*, 3766–3768.
Norman, D., Abuaf, P., Hingerty, B. E., Live, D., Grunberger, D., Broyde, S., & Patel, D. J. (1989) *Biochemistry 28*, 7462–7476.
Patel, D. J., Kozlowski, S. A., Nordheim, A., & Rich, A. (1982) *Proc. Natl. Acad. Sci. U.S.A. 79*, 1413–1417.
Patel, D. J., Shapiro, L., & Hare, D. (1987) *Q. Rev. Biophys. 20*, 35–112.
Reid, B. R. (1987) *Q. Rev. Biophys. 20*, 1–34.
Roche, C. J., Geacintov, N. E., Ibanez, V., & Harvey, R. G. (1989) *Biophys. Chem. 33*, 277–288.
Roche, C. J., Jeffrey, A. M., Mao, B., Alfano, A., Kim, S. K., Ibanez, V., & Geacintov, N. E. (1991) *Chem. Res. Toxicol. 4*, 311–317.
Schlick, T., Hingerty, B. E., Peskin, C. S., Overton, M. L., & Broyde, S. (1990) in *Theoretical Chemistry and Molecular Biophysics* (Beveridge, D., Live, D., & Lavery, R., Eds.) pp 39–58, Academic Press, New York.
Seiler, J. P. (1990) *Mutat. Res. 245*, 165–169.
Singer, B., & Grunberger, D. (1983) *Molecular Biology of Mutagens and Carcinogens*, Plenum Press, New York.
Singh, S. S., Hingerty, B. E., Singh, U. C., Greenberg, J. P., Geacintov, N. E., & Broyde, S. (1991) *Cancer Res. 51*, 3482–3492.
Slaga, T. J., Bracken, W. J., Gleason, G., Levin, W., Yagi, H., Jerina, D. M., & Conney, A. H. (1979) *Cancer Res. 39*, 67–71.
Stevens, C. W., Bouck, N., Burgess, J. A., & Fahl, W. E. (1985) *Mutat. Res. 152*, 5–14.
Testa, B. (1989) *Chirality 1*, 7–9.
van der Ven, F. J., & Hilbers, C. W. (1988) *Eur. J. Biochem. 178*, 1–38.
Weinstein, I. B., Jeffrey, A. M., Jennette, K. W., Blobstein, S. H., Harvey, R. G., Harris, C., Autrup, H., Kasai, H., & Nakanishi, K. (1976) *Science 193*, 592–594.
Wood, A. W., Chang, R. L., Levin, W., Yagi, H., Thakker, D. R., Jerina, D. M., & Conney, A. H. (1977) *Biochem. Biophys. Res. Commun. 77*, 1389–1396.
Zinger, D., Geacintov, N. E., & Harvey, R. G. (1987) *Biophys. Chem. 27*, 131–138.